



# Investigation of the parameters used in fused deposition modeling of poly (lactic acid) to optimize 3D printing sessions

E. Carlier<sup>a,\*</sup>, S. Marquette<sup>b</sup>, C. Peerboom<sup>b</sup>, L. Denis<sup>b</sup>, S. Benali<sup>c</sup>, J-M. Raquez<sup>c</sup>, K. Amighi<sup>a</sup>, J. Goole<sup>a</sup>

<sup>a</sup> Laboratory of Pharmaceutics and Biopharmaceutics, Université libre de Bruxelles, Faculty of Pharmacy, Brussels 1050, Belgium

<sup>b</sup> Laboratory UCB Pharma, Biological Formulation Development Group, Braine-l'Alleud, Belgium

<sup>c</sup> Laboratory of Polymeric and Composite Materials, UMONS, Mons, Belgium

## ARTICLE INFO

### Keywords:

3D printing  
Fused deposition modeling  
Thermomechanical properties  
Printing parameters  
Poly(lactic acid)

## ABSTRACT

This study assesses the feasibility of printing implantable devices using 3D printing Fused deposition modeling (FDM) technology. The influence of the deposition temperature, the deposition rate and the layer thickness on the printing process and the physical properties of the devices were evaluated. The filaments were composed of neat poly(lactic acid) (PLA) and blends of different plasticizers (polyethylene glycol 400 (PEG 400), triacetin (TA), acetyltriethyl citrate (ATEC) and triethyl citrate (TEC)) at 10% (w/w). The assessment of thermo-mechanical characteristics and morphology of both filaments and devices (cylinders and dog bones) were performed. The influence of each parameter was evaluated using a design of experiment (DoE) and the significance of the results was discussed. A large amount of data about the evaluation of FDM process parameters are already available in the literature. However, specific insights needed to be increased into the impact of the use of PLA and plasticized PLA raw material on the feasibility of printing devices in three dimensions. To conclude, the ductility was improved with a high layer thickness, low temperature and using ATEC. Whereas, adhesion was promoted with an increase in temperature, a lower layer thickness and adding TA.

## 1. Introduction

Fused deposition modeling (FDM) is a type of additive manufacturing technology that allows the production of three-dimensional (3D) devices from a computer-aided design (CAD) file (Carneiro et al., 2015; Jin et al., 2015). FDM is a user-friendly, adaptable, low-cost technique to quickly print prototypes with complex geometry (Kantaros and Karalekas, 2013; Panda et al., 2017). However, the FDM technique is characterized by some limitations due to its use of high temperatures. These temperatures may lead to potential thermal degradation, shrinkage issues, low surface quality and poor resolution. Such issues drastically limit the number of thermoplastic polymers that can be used, as well as the mixture of these with plasticizers when a decrease in their glass transition temperature ( $T_g$ ) is needed to reduce the printing

temperature (Alhnan et al., 2016; Bhushan and Caspers, 2017).

Moreover, although FDM is a fairly well-known 3DP technique, it is still a complex process to understand and control. This complexity is due to the relatively high number of parameters that may be modulated as well as their interdependence on the physicochemical properties of the final printed device. As these parameters are set during the design step (pre-processing) and remain constant throughout the printing process, it is still difficult to determine the appropriate parameters to obtain the desired rendering (Mohamed et al., 2016). Several studies have focussed on the optimization of the FDM process parameters, including mechanical properties and the anisotropic behaviour of thermoplastic materials during their extrusion through the nozzle (Afrose et al., 2016; Costa et al., 2017; Tymrak et al., 2014). Indeed, previous works have demonstrated that tensile parameters such as build

**Abbreviations:**  $\chi_c$ , degree of crystallinity; 3DP, three-dimensional printing; ABS, acrylonitrile butadiene styrene; ASTM, American Society for Testing and Materials; ATEC, acetyltriethyl citrate; CAD, computer-aided design; DoE, design of experiment; DSC, differential scanning calorimetry; EVA, ethylene vinyl acetate; FDM, fused deposition modeling; HME, hot melt extrusion; MFI, melt flow index; MPa, megapascal; Mw, molecular weight; PCL, poly( $\epsilon$ -caprolactone); PEG 400, polyethylene glycol 400; PLA, poly(lactic acid); PVA, polyvinyl alcohol; RP, rapid prototyping; rpm, revolutions per minute; SEM, scanning electron microscopy; SSE, single screw extruder; TA, triacetin; TEC, triethyl citrate;  $T_c$ , crystallization temperature;  $T_g$ , glass transition temperature; TGA, thermogravimetric analysis;  $T_{HME}$ , hot melt extrusion temperature;  $T_m$ , melting temperature; % (w/w), weight percentage

\* Corresponding author.

E-mail address: [emeric.carlier@ulb.ac.be](mailto:emeric.carlier@ulb.ac.be) (E. Carlier).

<https://doi.org/10.1016/j.ijpharm.2019.05.008>

Received 10 February 2019; Received in revised form 5 April 2019; Accepted 4 May 2019

Available online 06 May 2019

0378-5173/ © 2019 Elsevier B.V. All rights reserved.

orientation, extrusion temperature, air gap, raster width and layer thickness may be considered as the critical parameters that need to be understood and controlled. This is because they may affect the tensile strength, the resolution and the build time of the printed object (Chacón et al., 2017; Mohamed et al., 2016; Pfeifer et al., 2016).

It has also been shown that the layer thickness is a parameter playing a crucial role in a product's morphology. Indeed, Jin and co-workers investigated the surface profile of printed devices and concluded that a desired side surface quality can be achieved by modifying the raster angle and the layer thickness (Jin et al., 2015). Furthermore, the mechanical properties of printed devices are highlighted in the literature as depending on the layer thickness but with controversial analysis (Chacón et al., 2017). Indeed, Tymrak et al. evaluated the influence of layer thickness (0.2–0.4 mm) on both tensile strength and elastic modulus with printed dog-bone devices. The group concluded that a higher tensile strength was reached with a lower layer thickness (Tymrak et al., 2014). In addition, Chacon et al. investigated the influence of layer thickness in the three possible printing orientations (flat, on-edge and upright). The authors stated that the tensile strength in the upright direction was higher when the layer thickness was increased. However, in the flat and on-edge orientations, the layer thickness had almost no influence (Chacón et al., 2017).

The deposition temperature has influenced the adhesion between two successive layers and the bond quality. Distortions and defects may appear due to the rapid cooling of the matter. During deposition, the temperature of the bottom layer increases to above the  $T_g$  of the thermoplastic polymer, with a fast decrease in the temperature following the displacement of the print head (Christiyan et al., 2016; Turner et al., 2014).

Currently, the most commonly used thermoplastic polymers in FDM are acrylonitrile butadiene styrene (ABS), poly(lactic acid) (PLA), polyvinyl alcohol (PVA), poly( $\epsilon$ -caprolactone) (PCL) and ethylene vinyl acetate (EVA) (Goyanes et al., 2015; Torres et al., 2016). Furthermore, the printability and the quality of the printed devices depend on the thermal properties and the melt flow behaviour of the polymer (Wang et al., 2018). PLA is characterized by a high stiffness and brittleness (Södergård and Stolt, 2002). Therefore, improvement of the thermo-mechanical and flow properties of the PLA by adding plasticizers is widespread (Kamaly et al., 2016; Patil et al., 2015; Xiao et al., 2012).

The aim of the present study was to assess the feasibility of printing devices by FDM technology. However, in contrast to the existing literature about in this research area, it was decided to systematically explore the effect of various parameters using a single thermoplastic polymer (PLA) combined with different commonly used plasticizers (e.g. TA, ATEC, TEC, PEG 400) at the same percentage (10% (w/w)). Two models of devices were experimented, the cylinders and the dog bones. A completed DoE was set to explore as far as possible the influence of the various parameters on the physical properties of the devices. This optimization and characterization study has been performed on placebo devices, with the perspectives of including different active drugs in a close future.

## 2. Materials and methods

### 2.1. Materials

Ingeo Biopolymer 2003D PLA in pellets (96% L-lactide;  $\rho = 1.24 \text{ g/cm}^3$ ; MFI = 6 g/10 min (210 °C/2.16 kg), supplied by NatureWorks LLC (Minnetonka, USA), was used as a model thermoplastic polymer. PEG 400 purchased from Merck® Millipore (Massachusetts, USA), TEC purchased from Alfa Aesar (Lancashire, UK), ATEC purchased from Sigma-Aldrich (Missouri, USA) and TA purchased from Sigma-Aldrich (Missouri, US) were used as plasticizers. Dichloromethane was supplied by VWR (Pennsylvania, USA).

**Table 1**

Extrusion temperature ( $T_{HME}$ ) and screw speeds of each blend (n = 3).

Samples	$T_{HME}$ (°C)	Screw speeds (rpm)
Pure PLA	180	20
PLA – 10% (w/w) PEG 400	135	30
PLA – 10% (w/w) TEC	148	37
PLA – 10% (w/w) ATEC	137	22
PLA – 10% (w/w) TA	142	30

### 2.2. Methods

#### 2.2.1. Plasticized polymer blend

The commercial PLA pellets were dried overnight in a vented oven at 60 °C. In a flask, 30 g of PLA was placed with 300 mL of dichloromethane solution containing plasticizers until complete dissolution (adapted from (Baiardo et al., 2003) solvent casting method). Plasticizers were fixed at 10% (w/w) in the mixture materials. Polymer-plasticizer blends were placed under a ventilated hood before being dried for three days in an ventilated oven at 60 °C. Then, the mixtures were roughly cut and ground in nitrogen to obtain rough pellets (3–5 mm) which could be easily introduced into the extruder.

#### 2.2.2. Preparation of filaments by hot melt extrusion

Plasticized polymer filaments were prepared using a single screw extruder (SSE) (Noztek Touch, Noztek, Shoreham-by-Sea, UK) ( $\phi = 1.60 \text{ mm}$ ). For each extrusion, 15–20 g of blend was fed into the extruder. The extrusion was performed at a specified extrusion temperature and the speed of the screw was adapted for each blend (Table 1). After production, the diameter of the filament was checked every 5 cm in length using an electronic measuring calliper. Portions that did not have a diameter in the acceptable range of  $1.75 \pm 0.05 \text{ mm}$  were discarded. This was because the 3D printer was designed to process filaments with a diameter of 1.75 mm and only a small deviation of 0.05 mm could be tolerated without causing any issues. The filaments were stored in a vacuum desiccator prior to use.

#### 2.2.3. Device geometry

123D Design® (Autodesk®, California, USA) was used as the CAD program to design two models of devices, cylinders and dog bones, and to export them as .stl files. The specimen geometry followed the specifications outlined in ASTM D638-14 for type IV tensile specimens (Cantrell et al. 2011; ASTM D638, 2014; Kotlinski 2014). The cylindrical devices were designed with a diameter of 4 mm and a height of 40 mm. The dog-bone devices were characterized by an overall length of 115 mm, an overall width of 19 mm and a thickness of 4 mm (Fig. 1). All the printed devices were produced using a raft of 4.0 mm (raft margin) to stabilize the structure during the printing process. The raft of each structure was built using the minimal print rate of 1 mm/s available in the printer parameters, without a fan and with a minimum layer duration set at 15 s.

#### 2.2.4. Experimental design

FDM was performed by a MakerBot® Replicator 2 equipped with a 0.4 mm nozzle (MakerBot® Industries, New-York, USA). To investigate the mechanical properties (e.g. tensile strength, Young's modulus, elongation at break) of the printed dog bones and the weighing of the cylindrical devices, an experimental design was performed. Cylinders were characterized in terms of weight (Research RC 210P MC1 0.01 mg analytical balance; Sartorius, Göttingen, Germany; n = 3). The dog-bone devices were printed in an upright orientation to evaluate the adhesion between the layers, and followed the flat direction to evaluate the effect of the plasticizers on the mechanical properties. The design provided a fact-based approach, highlighting the printer performances, the relationship between variables and the influences of variables on a selected response. For these reasons, it was decided to perform first a

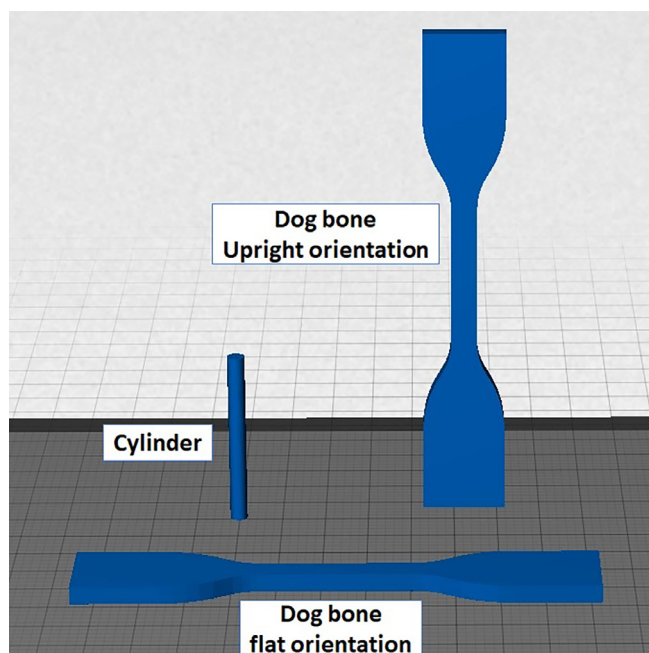


Fig. 1. Build orientations and shapes of the selected devices: a. cylinder 4 mm x 40 mm (diameter, height), b. dog bones 115 mm x 19 mm x 4 mm (overall length, overall width and thickness).

Table 2

Factors and levels applied in the experimental design.

Factors	Levels
Deposition temperature (°C)	155, 173, 190
Layer thickness (mm)	0.1, 0.2, 0.3
Deposition rate (mm/s)	1, 88, 175
Plasticizers	A TEC, PEG 400, TEC, TA

screening design to evaluate the principal effects of parameters before optimisation. The design was created using the JMP statistical software (SAS Institute Inc., North Carolina, USA). The factors and levels considered by the design for the 3D printing process are shown in Table 2: (1) the deposition temperature of the printing process were within the range 155 °C to 190 °C; (2) the deposition rate of the melt polymer on the build platform; (3) the layer thickness of the strand during the printing process, to evaluate its influence on the layer adherence and on the device morphology; (4) the influence of the plasticizer on the thermomechanical properties of the polymer and during the printing process. The impact of the evaluated factors was analysed using the least square regression method.

#### 2.2.5. Differential scanning calorimetry

DSC analyses were performed on a heat-flux type DSC Q2000 (TA instruments, Delaware, USA) equipped with a cooling system. Nitrogen gas was used as purge gas (flow rate = 50 mL/min) and data were collected with TA Instruments Universal Analysis 2000® software. Samples of 5–10 mg were introduced into TA aluminium pans and sealed with a lid (Tzero) made of the same material to evaluate the thermal properties (e.g. the glass transition temperature ( $T_g$ ), determined at the midpoint of the transitions; the cold crystallization temperature ( $T_c$ ); and the melting temperature ( $T_m$ ), determined as the midpoint temperature of the endotherms) of the filaments. The reference specimen consisted of an empty sealed pan. During the first cycle, the oven was heated from  $-20$  °C to 200 °C at 10 °C/min. During the second cycle, the samples were cooled to  $-20$  °C before being heated again to 200 °C at 10 °C/min.  $T_g$ ,  $T_c$  and  $T_m$  were captured during the second heating cycle. The degree of crystallinity ( $\chi_c$ ) was calculated

using the following equation (Eq. (1)):

$$\chi_c = \frac{\Delta H_m - \Delta H_c}{\Delta H_m^0} \times 100 \quad (1)$$

where  $\Delta H_m$  is the melting enthalpy,  $\Delta H_c$  is the enthalpy of cold crystallization achieved during the first heating cycle and  $\Delta H_m^0$  is the melting enthalpy of PLA 100% crystalline (93 J/g) (Farah et al., 2016). All the results were calculated using PLA quantity after subtraction of the 10% (w/w) of plasticizer.

#### 2.2.6. Thermogravimetric analysis (TGA)

The measurements were performed on a Q500 TGA (TA Instruments, Delaware, USA), equipped with a balance with a sensitivity of 0.1 µg. Nitrogen gas was used as purge gas (flow rate = 60 mL/min.). Samples of 5–8 mg were loaded into platinum pans to evaluate residual solvents (loss in mass) and to assess the thermal stability of both plasticizers and polymers. The climatic chamber was heated at 10 °C/min from 30 °C to 600 °C. Data collection and analysis were performed using TA Instruments® Universal Analysis 2000 software.

#### 2.2.7. Mechanical properties

The tensile testing was determined using a Lloyd LR 10 K (Ametek Inc, Pennsylvania, USA) with a load capacity of 10 kN. The 3D printed dog-bone specimens used for tensile tests were in accordance with the ASTM D638 (type IV). The reported values were the average of at least 3 measurements. The testing speed was set at 10 mm/min. Young's modulus, elongation at break (EB%) and tensile strength were obtained using NEXYGEN™ software (Ametek Inc, Pennsylvania, USA).

#### 2.2.8. Morphological analysis

The surface of the printed cylinder devices was visualized by scanning electron microscopy (SEM) using a JSM-600 scanning electron microscope (Jeol, Tokyo, Japan). They were fixed onto a carbon tape and coated with gold using a Balzers SCD 030 (Balzers Union Ltd., Liechtenstein).

#### 2.2.9. Melt flow index

A Davenport MFI-10 (Ametek, Pennsylvania, USA) melt flow indexer was used to evaluate the flowability of the melt. Material was cut into small pieces of around 5 mm before analysis. The ASTM standard test D1238 was used at 190 °C and a 2.16 kg load (ASTM D1238, 2013). MFI analyses were performed to evaluate the plasticizer effect on the PLA Ingeo 2003D viscosity and to correlate the amount of matter extruded during the printing process. The evaluation of the MFI was performed using two other temperatures following the DoE (173 and 155 °C) with a standard weight of a 2.16 kg load.

### 3. Results and discussion

#### 3.1. Formula and characteristics of the filament

The neat thermoplastic polymer PLA Ingeo 2003D was blended with the four previously-mentioned different plasticizers using a solvent evaporation method to obtain a homogeneous mixture before the extrusion process. The ratio of plasticizer (10% (w/w)) was considered miscible with the PLA after evaporation according to the miscibility study of Baiardo et al. (Baiardo et al., 2003). The researchers discussed about the miscibility of monomeric and polymeric plasticizers into the PLA. These plasticizer compounds were chosen because of their widespread use as plasticizers with PLA (Patil et al., 2015; Xiao et al., 2012). The addition of plasticizer is essential to soften the polymer, decrease its brittleness and enhance the processability of the polymer at relatively low process temperatures (Arrieta et al., 2014). Furthermore, the aim of this study was to transfer the knowledge acquired to the pharmaceutical formulation and thus to be able to reach the lowest

temperatures by adding plasticizers. TGA analysis was performed on the filaments to evaluate the residual amount of dichloromethane after extrusion. After three days in a ventilated oven at 60 °C, no loss of weight was observed above the boiling temperature of the solvent (~40 °C) (data not shown), which meant that it was completely removed. The complete elimination of the solvent inside the filament was shown to be essential as it was previously demonstrated that residual solvent may have a plasticizing effect (Verreck, 2012). To properly interpret the data from the DoE and the influence of the plasticizers on the printing process, it had to be certain that no interference would be generated by the presence of residual solvent. The plasticizer ratio was selected after experimental testing of different percentages (10, 20 and 30% (w/w)). With percentages higher than 10% (w/w), the diameter of the extruded filament was not in the printability range of  $1.75 \pm 0.05$  mm. This result was probably due to the inherent limitation of the single-screw extruder. Interestingly, it was observed that the diameter of the filament was greatly influenced by the speed of the screw. Indeed, there were swelling issues, which is also called the “Barus effect”, when the screw speed increased. This phenomenon has been described in the literature and can be explained by the viscoelastic properties of polymer. When polymer goes through the die at a relatively high velocity, its macromolecules relax. This leads to an increase in the filament diameter upon leaving the die (Jani and Patel, 2015). When a higher ratio than 10% (w/w) of plasticizer was used, the cooling step became more important due to the decrease of viscosity of the extruded filament. With 10% (w/w) of plasticizer, the aforementioned limitation of the filament diameter was achieved by adapting the SSE temperature and screw speed (Table 3). After the extrusion process, the filament was manually enrolled with a cylindrical container. The cylindrical container was put in an oven at 60 °C for 5 min to guarantee a constant enrol state to facilitate the storage of the filaments.

As expected, the  $T_{HME}$  of the pure PLA was reduced from 180 °C to 135, 148, 137 and 142 °C after blending with PEG 400, TEC, ATEC and TA, respectively (Table 3). The lowest  $T_{HME}$  values of 135 and 137 °C were obtained with PEG 400 and ATEC, respectively. Previous work explained that the role of plasticizers is to increase the free volume and minimize the chain interactions in the polymer structure (Maiza et al., 2015). Interestingly, the PEG 400 and ATEC were the highest  $M_w$  compounds added to the PLA in this study. However, at 148 °C the decrease in the  $T_{HME}$  was lower with TEC compared to other blends. This was despite the polar interaction between the ester groups of polymer and citrate compounds, which ensures a good solubility of the blend (Maiza et al., 2015).

The thermal properties of the extruded filaments were investigated by DSC (Fig. 2). The thermograms showed endothermic transition ( $T_g$ ), an exothermic peak related to the cold crystallization ( $T_c$ ) and an endothermic peak ( $T_m$ ) of the material. The extruded pure PLA was characterized by a  $T_g$  at 53 °C, a  $T_c$  at 110 °C and a  $T_m$  at 146 °C. As expected, the  $T_g$  of the blends shifted to lower temperatures due to the addition of the plasticizers (Table 3). The highest decrease in  $T_g$  value was obtained with the addition of PEG 400 as it was lowered from 53 °C to 34 °C. Furthermore, the addition of plasticizer in the thermoplastic polymer induced higher chain mobility and so a faster crystallization rate during the second heating cycle (Fig. 2) (Martin and Avérous, 2001).

**Table 3**

Extrusion temperature ( $T_{HME}$ ) and screw speed (rpm),  $T_g$ ,  $T_c$ ,  $\Delta H_c$ ,  $T_m$ ,  $\Delta H_m$  and ( $\chi_c$ ) for neat and plasticized PLA samples.

Samples	$T_{HME}$ (°C)	Screw speeds (rpm)	$T_g$ (°C)	$T_c$ (°C)	$\Delta H_c$ (J/g <sub>PLA</sub> )	$T_m$ (°C)	$\Delta H_m$ (J/g <sub>PLA</sub> )	( $\chi_c$ ) (%)
Pure PLA	180	20	53	110	25	150	28	3
PLA – 10% (w/w) ATEC	137	22	42	102	28	148	30	2
PLA – 10% (w/w) PEG 400	135	30	34	97	27	148	32	5
PLA – 10% (w/w) TA	142	30	40	99	27	147	29	2
PLA – 10% (w/w) TEC	148	37	40	98	25	147	30	5

However, the DSC cooling cycles showed no crystallization peak. The pure PLA and the blends are not able to crystallize at a cooling rate of 10 °C/min (Greco et al., 2018). The degree of crystallinity ( $\chi_c$ ) may be influenced by the thermomechanical properties of the PLA (Table 3). As observed, the crystallinity of the PLA (3%) increased when PEG 400 and TEC were added (5%). Chain mobility was promoted with the presence of plasticizer and explained this observation (Wang et al., 2014). Interestingly, a lower crystallinity was observed with the addition of ATEC and TA as plasticizers (2%).

In addition, the melting peak of both neat and plasticized PLA was not defined as a single peak but as a double peak. The literature reports that these melting peaks correspond to the crystalline structure ( $\alpha$ - and  $\alpha'$ -forms) of the PLA and the original crystalline structure recrystallization respectively by lamellar rearrangement (Fehri et al., 2016; Li et al., 2018).

The DSC thermograms showed an influence from the plasticizer on the  $T_g$  and the  $T_{HME}$  of the blend (Table 3). However, the variation in  $T_{HME}$  was influenced by the plasticizer and was not only dependent on the decrease in  $T_g$ . The  $T_{HME}$  was higher with the neat PLA and when the PLA was plasticized with TEC. These results were related to the higher viscosity of the matter in both situations.

TGA were performed on both neat and plasticized PLA filaments (Fig. 3). Indeed, the thermal stability of PLA after the addition of plasticizers could be modified due to the higher mobility of the polymer chains. It was observed that the mass of the sample started to decrease at lower temperatures when plasticizers were added compared to neat PLA. The weight loss curve derivatives (DTG) were analysed to assess the thermal stability of the filaments at the selected range of printing temperatures (155–190 °C). The DTG curves of both pure and plasticized PLA showed that degradation appeared above 200 °C (Fig. 3). However, the filament made of PLA and PEG 400 blend was less subject to degradation than those made of other plasticizers. The shift is more obvious if small molecules are added into the polymer matrix, due to their thermal stability. Furthermore, the thermal stability with the PEG 400 was higher than that from the use of the three other plasticizers (ATEC, TA, TEC). According to Li and co-workers, the shift was due to the degradation of the plasticizer when the initial temperature of degradation of the plasticizers was reached, and promoted the degradation of PLA (Li et al., 2018).

### 3.2. MFI analysis of the filaments

As recommended by Fuenmayor and co-workers, MFI analysis was performed to evaluate the ability of the matter to flow through the printer nozzle at the three selected temperatures: 155, 173 and 190 °C (Fuenmayor et al., 2018). The lowest temperature corresponds to that at which the devices can be printed at a minimum printing temperature adapted to all blends. The highest temperature corresponds to the temperature at which the devices can be printed just before the degradation of the filament begins, using TGA data. The MFI of the filaments were evaluated according to the ASTM D1238 norms. At 210 °C, the MFI provided by the manufacturer was 6 g/10 min. At 190 °C, the MFI of the pure PLA was found to be 7.29 g/10 min. At 173 °C, the MFI of raw PLA decreased even more to 3.67 g/10 min (Fig. 4). At 155 °C, PLA flowed at only 1.99 g/10 min. As shown, it was clearly

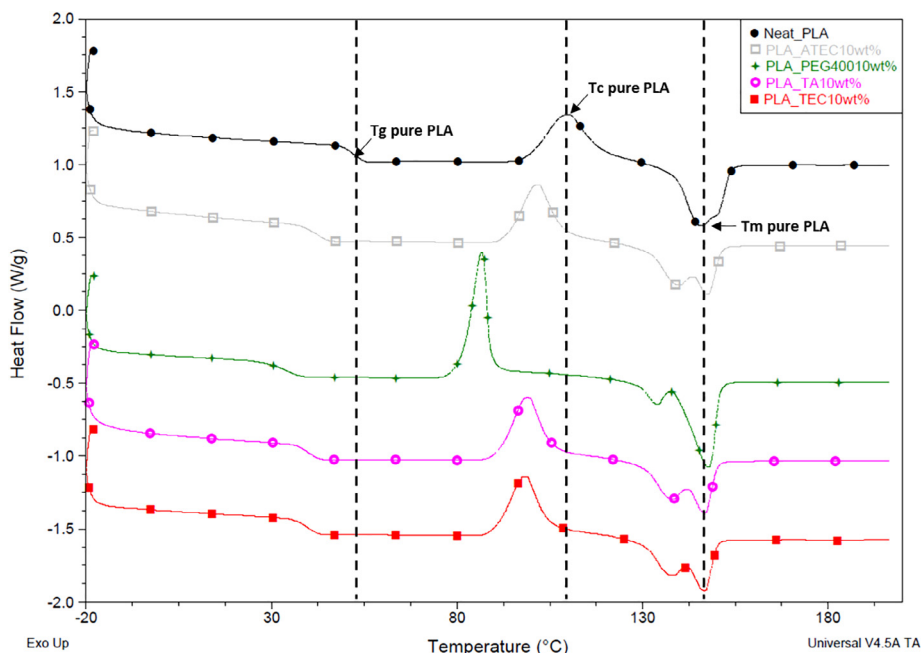


Fig. 2. Comparison of DSC thermograms of the neat PLA (●) and plasticized PLA with ATEC (■), TA (○), TEC (■) and PEG 400 (\*) captured during the second heating cycle.

demonstrated that the flowability of this thermoplastic polymer was reduced when the temperature was decreased.

Indeed, the addition of 10% (w/w) of plasticizer made it possible to obtain a flow of PLA at the three temperatures tested. Regardless of the temperature, the MFI were enhanced in comparison to that of pure PLA. However, the nature of the plasticizers influenced the flowing behaviour of the polymer (Fig. 4). Indeed, it was clearly demonstrated that the addition of PEG 400 increased the MFI to a greater extent than the values observed with the other plasticizers, regardless of the evaluated temperature (Fig. 4).

Recently, Wang and co-workers screened different commercial PLA and concluded that a MFI value of 10 g/10 min was necessary to obtain 3D devices with an acceptable quality between 190 and 220 °C (Wang et al., 2018). Furthermore, they highlighted that during the polymer melt deposition, the importance of the plasticizer and the crystallinity

need to be considered together, in addition to that of the MFI value (Wang et al., 2018). During this work, several values were lower than the expected 10 g/10 min. Interestingly, the addition of 10% (w/w) of plasticizer was slightly appreciable. The PLA MFI values at 155 °C increased from 1.99 g/10 min to 4.02, 3.66 and 3.12 g/10 min with ATEC, TA and TEC respectively. In contrast, a higher MFI value (25.02 g/10 min) was observed with PEG 400. Despite the difficulty in obtaining a structure without defects, the aim of the study was to achieve the results with a wide range of parameters. Furthermore, the wide range of parameters included the worst-case temperature of 155 °C.

### 3.3. Manufacture of the devices by FDM

The selected model of thermoplastic polymer was printed at 230 °C using the manufacturer’s specifications (Torres et al., 2016). With a

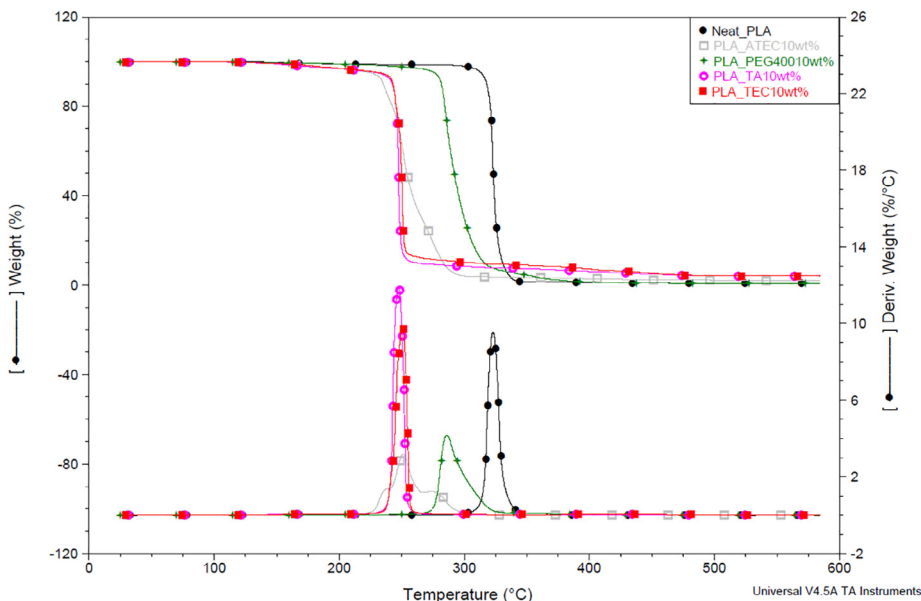


Fig. 3. Comparison of the TGA (above) and DTG (below) thermograms of the neat PLA (●) and plasticized PLA with ATEC (■), TA (○), TEC (■) and PEG 400 (\*).

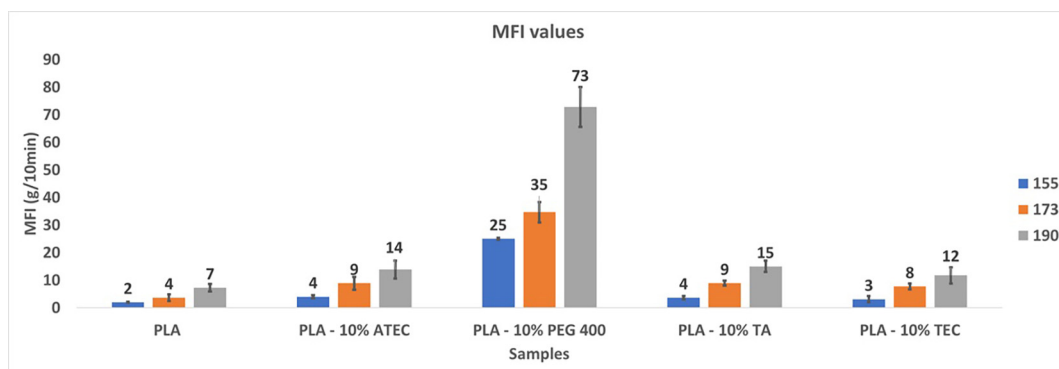


Fig. 4. MFI results (g/10 min) of the neat and plasticized PLA following the selected temperatures (155 °C (blue), 173 °C (orange), 190 °C (grey), n = 3).

view to developing further 3DP devices containing pharmaceutical active compounds, the addition of plasticizer makes it possible to decrease the printing temperature. To overcome the degradation which could take place during the printing session, the influence of several plasticizers on it were evaluated. Information concerning printing protocols for using plasticized material is lacking and could be interesting in the pharmaceutical field. In this case, the most rational approach to obtaining information about the process was to perform a DoE. The printing parameters and the plasticizer influence could easily be screened to identify a printing protocol that allows the production of adequate 3DP devices.

The experimental design was established with four parameters, in line with their available ranges and values. Each parameter was set with a minimal and a maximal value as well as an arithmetic mean thereof. The selected DoE was established to obtain information and understand the printability of the matter using a wide range of parameters (Table 4).

The estimation of the lower temperature was evaluated using an empirical method. The plasticized PLA filaments were tested at several loading temperatures. Furthermore, adhesion onto the platform was necessary to print devices. At the adhesion temperature, the loading of the filament could be performed without obstruction: the plasticized thermoplastic polymer flowed properly through the nozzle of the printer and adhered to the build platform, regardless of the plasticizer used. However, to enhance the adhesion of the devices onto the platform during the printing process, blue tape was systematically used (Skowrya et al., 2015). The maximal temperature was set at 190 °C to prevent the degradation of the filaments, in accordance with DTG data (Fig. 3).

Both the deposition rate (1–175 mm/s) and the layer thickness (0.1–0.3 mm) were fixed in accordance with the manufacturer's requirements. The infill of the devices was set at 100% to evaluate the

Table 4  
Experimental design used to produce the devices.

Experiments #	Deposition temperatures (°C)	Layer thicknesses (mm)	Deposition rates (mm/s)	Plasticizers (10% (w/w))
1	190	0.1	175	Triacetin
2	173	0.2	88	ATEC
3	155	0.3	1	Triacetin
4	155	0.1	175	TEC
5	190	0.1	1	ATEC
6	190	0.1	1	Triacetin
7	155	0.3	175	ATEC
8	155	0.1	1	PEG 400
9	190	0.3	175	PEG 400
10	173	0.2	88	TEC
11	190	0.3	1	TEC
12	173	0.2	88	PEG 400

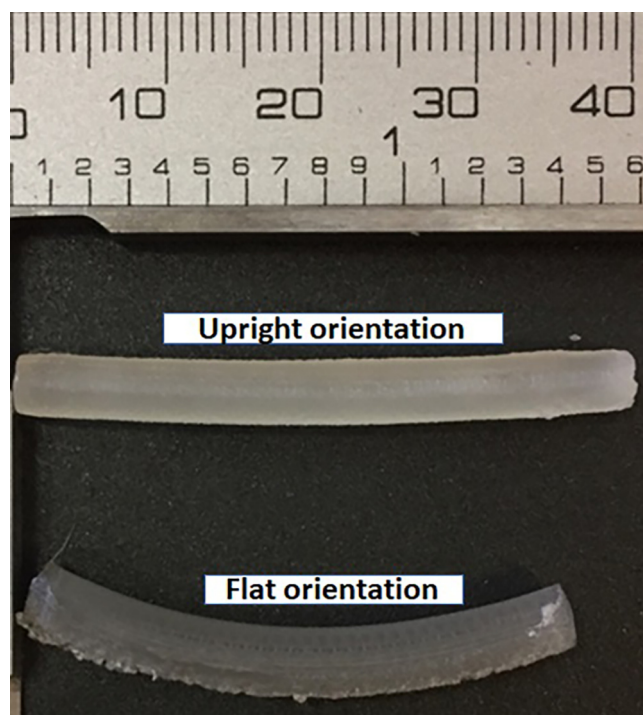
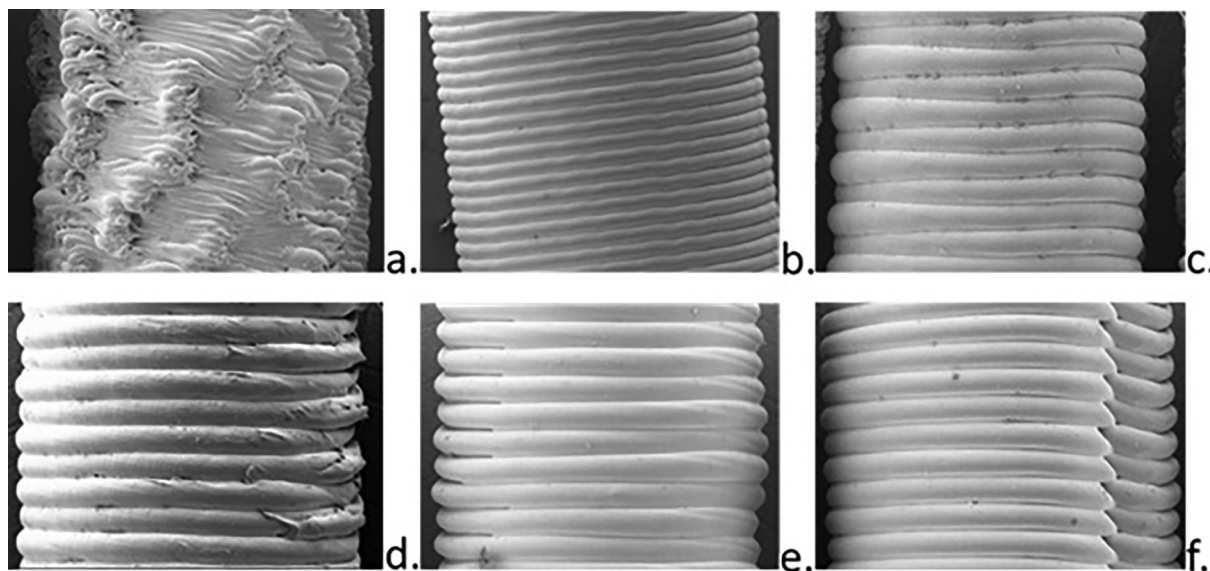


Fig. 5. Shrinkage of the cylinder device printed in the upright orientation and in the flat orientation (mm).

potential maximum response during the test.

During the first part of the investigation, the upright orientation was used for cylinder devices due to the high degree of shrinkage in the flat orientation (Fig. 5).

The printing process was performed using a raft (small horizontal lattice of melt filament laid down between the build platform and device) to increase the adhesion of the first layer onto the build platform and to improve the stability of the devices during the whole process. The raft played a key role in printing the cylinder devices and the dog bones in the upright orientation. Indeed, due to the small area of contact between their bases (12.56 mm<sup>2</sup>) and the build platform, both devices pitched during the printing until they were completely peeled off by the repeated back-and-forth movement of the print head. As previously described by Carneiro and co-workers, the nozzle of the 3D printer was manually adjusted at 0.36 mm to the platform and so expanded the extrusion width to enhance the overlapping of the layers of the raft (Carneiro et al., 2015). Such manual adjustment of the nozzle did not interact with the printability of the devices as the build platform moved down by increments to provide the right preselected layer height.



**Fig. 6.** SEM micrographs of the surface of cylindrical devices with: a. sample 8 (155 °C, 0.1 mm, 1 mm/s), b. sample 2 (173 °C, 0.2 mm, 88 mm/s), c. sample 7 (155 °C, 0.3 mm, 175 mm/s), d. sample 3 (155 °C, 0.3 mm, 1 mm/s), e. sample 9 (190 °C, 0.3 mm, 175 mm/s), f. sample (190 °C, 0.3 mm, 1 mm/s) at 30x magnification.

### 3.4. Morphological analysis of the printed cylinder devices

SEM analysis was performed on the samples to get more insight into the morphology of the external surfaces of the printed devices (Fig. 6b). The layer height modulation at three different levels (0.1, 0.2, 0.3 mm) could have an influence on the surface of the devices. Fig. 6 shows the comparison of the external surface SEM micrograph of samples 2, 3, 7, 8, 9 and 11, obtained following the different layer heights. As hypothesized, the increase in the height had a positive influence on the resolution of the devices. At 0.1 mm (Fig. 6a), the matter was highly embedded, most probably because the build platform went down slowly, and the printer nozzle had an extended contact area during the process. The improvement of the morphology was due to the increase in the thickness to reach values of 0.2 and 0.3 mm. Interestingly, the external surface of sample 7 (Fig. 6c), which was printed at a temperature of 155 °C and at 175 mm/s, is faithful to the design, while the MFI of the initial filament (PLA\_ATEC10% (w/w)) was only 3.42 g/10 min. A better resolution may be important in the future when developing pharmaceutical dosage forms to promote a high surface area and avoid the solid-state surface obtained with 0.1 mm of layer height.

### 3.5. Design of experiment

The experimental design was performed to investigate the printability of the matter following a set of four parameters. To our knowledge, these parameters included four different plasticizers that have not already been investigated for 3DP. To visualize the effect of each parameter and the associated response, a prediction profiler was used (Fig. 7). The prediction profiler provided an overview of the responses before the discussion below, based on each effect. Furthermore, the profile can be employed to estimate the response of each experimental parameter.

### 3.6. The effect of the FDM process parameters on the weight of the cylinder devices

It has been demonstrated that the deposition temperature, the layer thickness and the plasticizers had a significant impact on the variability of the mass of the devices after printing ( $p < 0.05$ ) (Fig. 7). This result may be correlated with the flow of the matter through the nozzle. The

weight of the cylindrical devices increased when the deposition temperature was raised.

When the temperature rose, the flow through the nozzle increased, which was confirmed by the MFI values (Fig. 4). Higher temperatures (173 and 190 °C) led to avoidance of nozzle clogging and improved the regularity of the polymer rods on the platform. In contrast, an increase in the layer thickness showed a negative influence on the weight at values higher than 0.1 mm. Chacon and co-workers explained that when the layer thickness increased, a lower number of layers was needed to achieve the final structure (Chacón et al., 2017). Therefore, the printed devices with higher thicknesses needed less material and so were characterized by a lower weight. This observation could be attractive to adapt the loading percentage of an active molecule to a 3DP drug delivery system. The influence of the addition of plasticizers on the weight was unexpected. Indeed, although the addition of PEG 400 to the PLA increased its MFI, it seemed that the flow of the mass was lower during the printing with this plasticizer.

### 3.7. The effect of the FDM parameters on the mechanical properties of the dog-bone devices

As recommended by Abdelwahab and co-workers, mechanical testing was performed on both neat and plasticized PLA dog-bone devices (Abdelwahab et al., 2012). The brittleness behaviour of the PLA is widely known and enhancement of the mechanical properties of the material was required. The ductility of the 3DP devices was improved by the addition of plasticizers (Arrieta et al., 2014; Farah et al., 2016; Jin et al., 2017; Södergård and Stolt, 2002). It was previously demonstrated that PLA is characterized by a high Young's modulus and tensile strength (Baiardo et al., 2003). It was expected that the addition of plasticizers could decrease both Young's modulus and tensile strength values, with an increase in the elongation at break values of PLA. The devices were printed following the upright and the flat orientations. The flat orientation was used as typical shape to investigate the mechanical properties of the material. The adhesion between the layers was investigated on devices that were printed in the upright orientation. Furthermore, the experiments showed that the flat orientation resulted in difficulties such as shrinkage and defects in obtaining cylindrical devices. Hence, the main approach to produce devices was to print in the upright orientation. The evaluation of the anisotropy of the

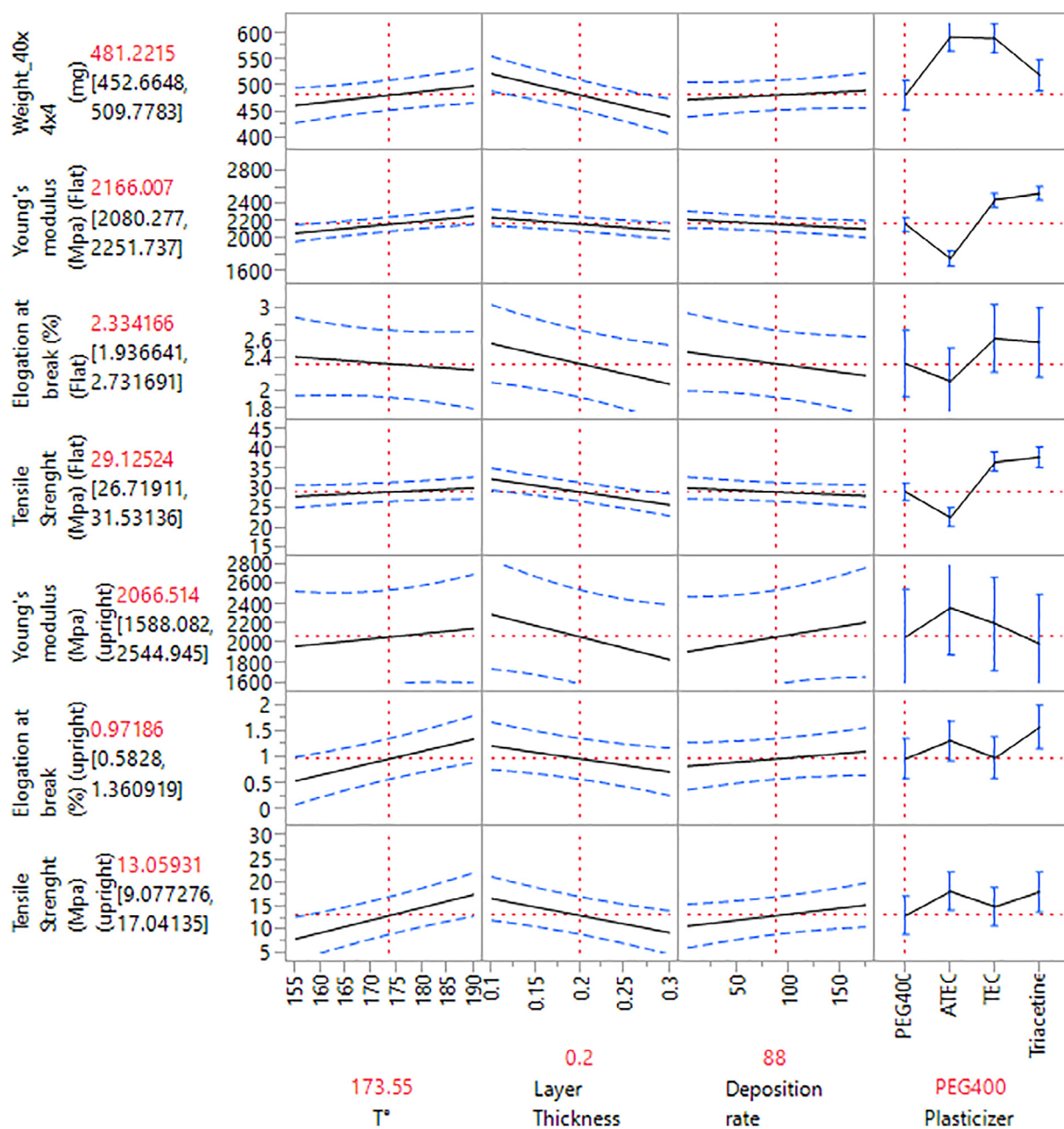


Fig. 7. Summary of the effect of the evaluated parameters (deposition temperature ( $T^*$ ), layer thickness, deposition rate and type of plasticizer) on the analysed factors (weight, Young's modulus, elongation at break and tensile strength) generated during the experiments with a prediction profiler. The estimate values (y-axis, red) of those factors are according to the fixed parameters (x-axis, red).

mechanical response of the 3DP devices could improve the ability to print devices in the upright orientation and promote a similar structure to that initially designed. Chacon and co-workers showed that the tensile strength of a printed device could be modulated by varying only the orientation of the printing. Indeed, it was demonstrated that the tensile testing was performed parallel to the layer deposition in the case of upright samples. This observation was contrary to the one demonstrated to the flat-oriented devices. Moreover, these results were in accordance to the literature (Chacón et al., 2017).

The tensile test was performed to evaluate the Young's modulus, the elongation at break and the tensile strength of the dog-bone devices.

The deposition temperature significantly modified the Young's modulus ( $p = 0.004$ ) with the flat oriented dog bones. It was observed that an increase in the deposition temperature led to higher Young's modulus values (Fig. 8a). Indeed, considering the temperature range

from 155 °C to 190 °C, the Young's modulus was able to increase from  $1556.6 \pm 557.8$  MPa to  $2786.4 \pm 147.7$  MPa for experiments 6 and 7, respectively (Table 4). For the upright orientation, the responses were significant for the elongation at break ( $p = 0.007$ ) and for the tensile strength ( $p = 0.004$ ) (Fig. 8a and b). The higher temperature tended to promote an increase in both mechanical properties. Indeed, the elongation at the break maximum value of  $2.6 \pm 0.4\%$  was observed during experiment 1 (Table 4). The tensile strength increased from  $6.8 \pm 2.2$  MPa to  $28.2 \pm 1.1$  MPa in the range of temperatures 155–190 °C. Torres et al. stated that when the temperature was increased, the molten state of the PLA led to a better adhesion to the previous layer (Torres et al., 2016). The tensile strength of the upright-printed pure PLA following the manufacturer requirements at 230 °C, 90 mm/s was  $19.9 \pm 0.5$  MPa and  $47.5 \pm 2.4$  MPa, with a layer thickness of 0.1 and 0.3 mm respectively. These values highlighted that

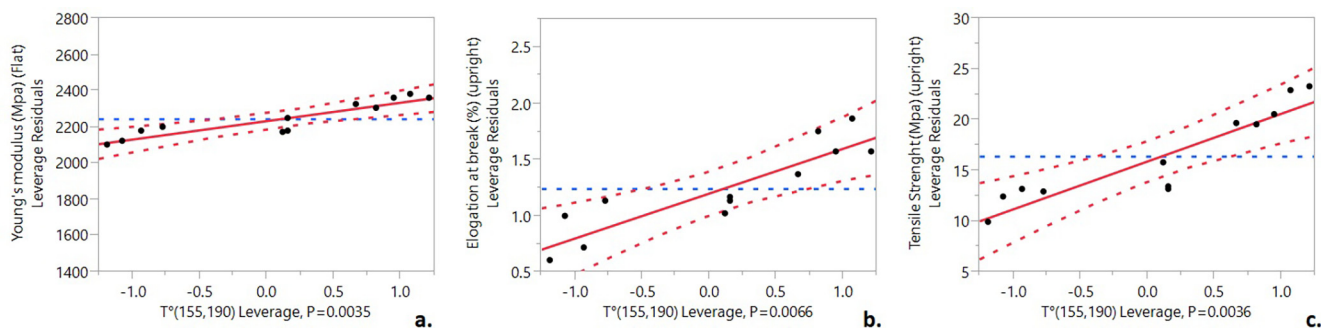


**Fig. 8.** Tendency of the deposition temperature for: a. the Young's modulus in the flat orientation, b. the elongation at break in the upright orientation, c. the tensile strength in the upright orientation.

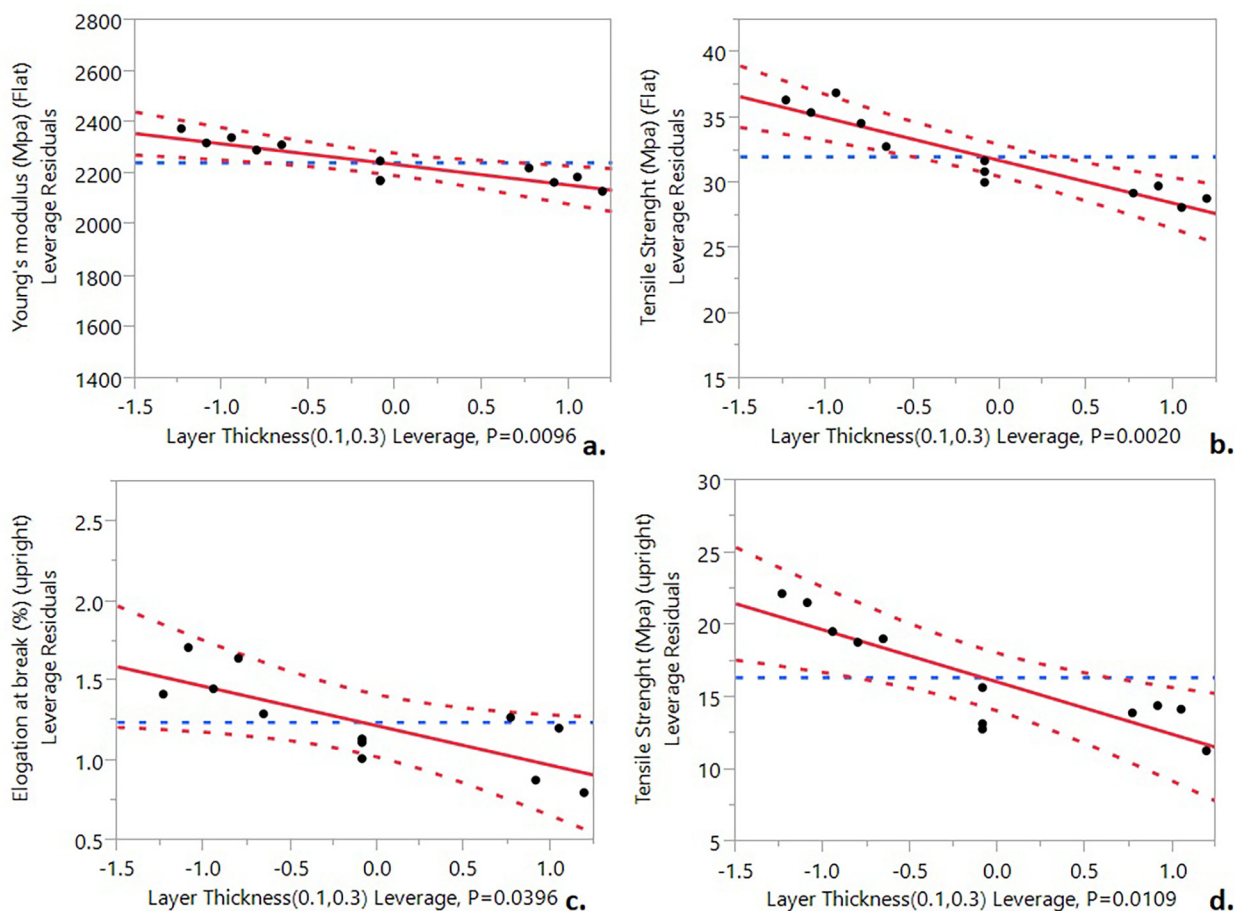


**Fig. 9.** Tendency of the layer thickness for: a. Young's modulus in the flat orientation, b. the tensile strength in the flat orientation, c. the elongation at break in the upright orientation, d. the tensile strength in the upright direction.

the decrease in temperature succeeded in producing 3DP devices, regardless of the thickness of the layers.

The layer thickness significantly affected both Young's modulus ( $p = 0.01$ ) and tensile strength ( $p = 0.002$ ) in the flat orientation as well as both elongation at break ( $p = 0.04$ ) and tensile strength ( $p = 0.01$ ) following the upright orientation (Fig. 9). Regardless of the printing orientation, an increase in the layer thickness led to lower mechanical properties. Indeed, all the mechanical properties tended to decrease when the layer thickness increased from 0.1 to 0.3 mm. The decrease in the Young's modulus values when the layer thickness increased led to a decrease in the stiffness of the device (Fig. 9a). Indeed, the stiffness of the matter was evaluated following the Young's modulus values (Chacón et al., 2017). The decrease in both Young's modulus and tensile strength led to a lower stiffness of the material. Tymrak and co-

workers highlighted a similar trend in their work on PLA. Indeed, a higher tensile strength was reached by lowering the layer thickness (Tymrak et al., 2014). When the devices were printed in the upright orientation, the tendency was similar to that previously mentioned. A higher layer thickness tended to promote lower mechanical properties (Fig. 9c and d). Interestingly, Chacon and co-workers found that the upright strength increased with a higher layer thickness. Moreover, in the flat orientation, the decrease in the layer thickness increased the strength but with only a slight effect (Chacón et al., 2017). This result was different from that obtained during our experiments. In Chacón et al.'s study, the effects of layer thickness, build orientation and feed rate on PLA printed devices were evaluated for the PLA mechanical properties. In the case of the present study, the deposition temperature was modulated and plasticizers were added. However, the design of

experiment was performed to evaluate the main effect of the selected FDM parameters.

The deposition rate was the printing parameter with the least influence on the mechanical properties (Fig. 7). Indeed, the only significant response was a slight decrease in the Young's modulus ( $p = 0,04$ ) when the devices were printed in the flat orientation. Consequently, it may be interesting to evaluate the interaction between the deposition temperature and the deposition rate as this could explain the previous statement. A lower deposition temperature (155 °C) associated with a higher deposition rate (175 mm/s) can lead to more porous structures due to a lack of the intra-layer adhesion during the process (Christiyan et al., 2016).

The influence of the plasticizer on the mechanical properties was also investigated on dog bones. The significance of the results was different according to the orientation of the printing. The model responses were significant only when both Young's modulus and tensile strength values were lower than the two significant model responses. ATEC was shown to be the most significant influencing plasticizers on a decrease in both Young's modulus and tensile strength ( $p < 0.0001$ ) (Fig. 7). The addition of ATEC in PLA led to a sharp decrease in its stiffness and increased its ductility. In contrast, the addition of TEC and TA to the polymer matrix increased both Young's modulus and tensile strength in the flat orientation. PEG 400 had no significant effect on the Young's modulus and had a slight effect on the tensile strength, in the same orientation. When the dog bones were printed in upright orientation, the nature of the plasticizers had a lower influence on the mechanical properties. The only significant response was obtained for the elongation at break. Moreover, the TA was the only plasticizer that had a significant effect on the elongation at break. An increase in the elongation at break was observed when TA was added.

#### 4. Conclusion

This study showed that the addition of ATEC seems to reduce the PLA stiffness and the addition of TA promotes a better adhesion between layers. Furthermore, the stiffness of the material can also be modulated by the choice of parameters and the printing orientation. Indeed, the ductility was improved by a higher layer thickness, while a lower deposition temperature led to a less stiff material and consequently to a harmless implant for the patient. The adhesion between layers was promoted by a decrease in layer thickness and an increase in the deposition temperature. No significant effect on the deposition rate was observed with the selected DoE. The interrelationship between parameters needs to be investigated to improve knowledge about the mechanical properties of the plasticized PLA and the influence of the printing parameters.

In addition, it could be interesting to understand how the matter reacts during and after the FDM process to perform flexural testing. The orientation had a key role on the mechanical results, but the selected raster angle should be evaluated due to its ability to increase the load-bearing behaviour of the fibres deposited by the printhead. Furthermore, the addition of an active molecule into the polymer matrix will modify the structure as well as the thermomechanical properties.

#### Declaration of Competing Interest

The authors declare that they have no known competing financial interests or personal relationships that could have appeared to influence the work reported in this paper.

#### Acknowledgement

The authors would like to thank UCB Pharma and the Walloon region for providing funding to make this study possible and also thank Mr Madau P. who provided technical assistance for the scanning

electron microscopy.

#### References

- Abdelwahab, M.A., Flynn, A., Sen Chiou, B., Imam, S., Orts, W., Chiellini, E., 2012. Thermal, mechanical and morphological characterization of plasticized PLA-PHB blends. *Polym. Degrad. Stab.* 97, 1822–1828. <https://doi.org/10.1016/j.polymdegradstab.2012.05.036>.
- Afrose, M.F., Masood, S.H., Iovenitti, P., Nikzad, M., Sbarski, I., 2016. Effects of part build orientations on fatigue behaviour of FDM-processed PLA material. *Prog. Addit. Manuf.* 1, 21–28. <https://doi.org/10.1007/s40964-015-0002-3>.
- Alhnan, M.A., Okwuosa, T.C., Sadia, M., Wan, K.W., Ahmed, W., Arafat, B., 2016. Emergence of 3D printed dosage forms: opportunities and challenges. *Pharm. Res.* <https://doi.org/10.1007/s11095-016-1933-1>.
- Arrieta, M.P., Castro-López, M.D.M., Rayón, E., Barral-Losada, L.F., López-Vilariño, J.M., López, J., González-Rodríguez, M.V., 2014. Plasticized poly(lactic acid)-poly(hydroxybutyrate) (PLA-PHB) blends incorporated with catechin intended for active food-packaging applications. *J. Agric. Food Chem.* 62, 10170–10180. <https://doi.org/10.1021/jf5029812>.
- ASTM, 2014. ASTM D638 – 14. Standard Test Method for Tensile Properties of Plastics. *Ann. B. ASTM Stand.* 1–20. <https://doi.org/10.1520/D0638-14>.
- ASTM D1238, 2013. ASTM D1238 – Standard Test Method for Melt Flow Rates of Thermoplastics by Extrusion Plastometer. *Ann. B. ASTM Stand.* 1–16. doi: 10.1520/D1238-13.
- Baiardo, M., Frisoni, G., Scandola, M., Rimelen, M., Lips, D., Ruffieux, K., Wintermantel, E., 2003. Thermal and mechanical properties of plasticized poly(L-lactic acid). *J. Appl. Polym. Sci.* 90, 1731–1738. <https://doi.org/10.1002/app.12549>.
- Bhushan, B., Caspers, M., 2017. An overview of additive manufacturing (3D printing) for microfabrication. *Microsyst. Technol.* 23, 1117–1124. <https://doi.org/10.1007/s00542-017-3342-8>.
- Cantrell, J., Rohde, S., Damiani, D., Gurnani, R., Disandro, L., Anton, J., Young, A., Jerez, A., Steinbach, D., Kroese, C., Ifju, P., 2011. Experimental characterization of the mechanical properties of 3d-printed abs and polycarbonate parts. *Univ. Florida* 89–105. [https://doi.org/10.1007/978-3-319-41600-7\\_11](https://doi.org/10.1007/978-3-319-41600-7_11).
- Carneiro, O.S., Silva, A.F., Gomes, R., 2015. Fused deposition modeling with polypropylene. *Mater. Des.* 83, 768–776. <https://doi.org/10.1016/j.matdes.2015.06.053>.
- Chacón, J., Caminero, M., García-Plaza, E., Núñez, P., 2017. Additive manufacturing of PLA structures using fused deposition modelling: effect of process parameters on mechanical properties and their optimal selection. *Mater. Des.* 124, 143–157. <https://doi.org/10.1016/j.matdes.2017.03.065>.
- Christiyan, K.G.J., Chandrasekhar, U., Venkateswarlu, K., 2016. A study on the influence of process parameters on the Mechanical Properties of 3D printed ABS composite. 012109. *IOP Conf. Ser. Mater. Sci. Eng.* 114. <https://doi.org/10.1088/1757-899X/114/1/012109>.
- Costa, S.F., Duarte, F.M., Covas, J.A., 2017. Estimation of filament temperature and adhesion development in fused deposition techniques. *J. Mater. Process. Technol.* 245, 167–179. <https://doi.org/10.1016/j.jmatprotec.2017.02.026>.
- Farah, S., Anderson, D.G., Langer, R., 2016. Physical and mechanical properties of PLA, and their functions in widespread applications – a comprehensive review. *Adv. Drug Deliv. Rev.* 367–392. <https://doi.org/10.1016/j.addr.2016.06.012>.
- Fehri, S., Cinelli, P., Coltelli, M.-B., Anguillesi, I., Lazzari, A., 2016. Thermal properties of plasticized poly (Lactic Acid) (PLA) containing nucleating agent. *Int. J. Chem. Eng. Appl.* 7, 85–88. <https://doi.org/10.7763/IJCEA.2016.V7.548>.
- Fuenmayor, E., Forde, M., Healy, A.V., Devine, D.M., Lyons, J.G., McConville, C., Major, I., 2018. Material considerations for fused-filament fabrication of solid dosage forms. *Pharmaceutics* 10. <https://doi.org/10.3390/pharmaceutics10020044>.
- Goyanes, A., Robles Martínez, P., Buanz, A., Basit, A.W., Gaisford, S., 2015. Effect of geometry on drug release from 3D printed tablets. *Int. J. Pharm.* 494, 657–663. <https://doi.org/10.1016/j.ijpharm.2015.04.069>.
- Greco, A., Ferrari, F., Maffezzoli, A., 2018. Thermal analysis of poly(lactic acid) plasticized by cardanol derivatives. *J. Therm. Anal. Calorim.* 1–7. <https://doi.org/10.1007/s10973-018-7059-4>.
- Jani, R., Patel, D., 2015. Hot melt extrusion: an industrially feasible approach for casting orodispersible film. *Asian J. Pharm. Sci.* 10, 292–305. <https://doi.org/10.1016/j.ajps.2015.03.002>.
- Jin, Y., Wan, Y., Zhang, B., Liu, Z., 2017. Modeling of the chemical finishing process for polylactic acid parts in fused deposition modeling and investigation of its tensile properties. *J. Mater. Process. Technol.* 240, 233–239. <https://doi.org/10.1016/j.jmatprotec.2016.10.003>.
- Jin, Y.A., Li, H., He, Y., Fu, J.Z., 2015. Quantitative analysis of surface profile in fused deposition modelling. *Addit. Manuf.* 8, 142–148. <https://doi.org/10.1016/j.addma.2015.10.001>.
- Kamaly, N., Yameen, B., Wu, J., Farokhzad, O.C., 2016. Degradable controlled-release polymers and polymeric nanoparticles: Mechanisms of controlling drug release. *Chem. Rev.* <https://doi.org/10.1021/acs.chemrev.5b00346>.
- Kantaros, A., Karalekas, D., 2013. Fiber Bragg grating based investigation of residual strains in ABS parts fabricated by fused deposition modeling process. *Mater. Des.* 50, 44–50. <https://doi.org/10.1016/j.matdes.2013.02.067>.
- Kotlinski, J., 2014. Mechanical properties of commercial rapid prototyping materials. *Rapid Prototyp. J.* 20, 499–510. <https://doi.org/10.1108/RPJ-06-2012-0052>.
- Li, D., Jiang, Y., Lv, S., Liu, X., Gu, J., Chen, Q., Zhang, Y., 2018. Preparation of plasticized poly (lactic acid) and its influence on the properties of composite materials. *PLoS One* 13, 1–15. <https://doi.org/10.1371/journal.pone.0193520>.
- Maiza, M., Benaniba, M.T., Quintard, G., Massardier-Nageotte, V., 2015. Biobased additive plasticizing Poly(lactic acid) (PLA). *Polimeros* 25, 581–590. <https://doi.org/10.1007/s10973-018-7059-4>.

- 1590/0104-1428.1986.
- Martin, O., Avérous, L., 2001. Poly(lactic acid): Plasticization and properties of biodegradable multiphase systems. *Polymer (Guildf)* 42, 6209–6219. [https://doi.org/10.1016/S0032-3861\(01\)00086-6](https://doi.org/10.1016/S0032-3861(01)00086-6).
- Mohamed, O.A., Masood, S.H., Bhowmik, J.L., 2016. Optimization of fused deposition modeling process parameters for dimensional accuracy using I-optimality criterion. *Measurement* 81, 174–196. <https://doi.org/10.1016/j.measurement.2015.12.011>.
- Panda, B.N., Shankhwar, K., Garg, A., Jian, Z., 2017. Performance evaluation of warping characteristic of fused deposition modelling process. *Int. J. Adv. Manuf. Technol.* 88, 1799–1811. <https://doi.org/10.1007/s00170-016-8914-8>.
- Patil, H., Tiwari, R.V., Repka, M.A., 2015. Hot-melt extrusion: from theory to application in pharmaceutical formulation. *AAPS PharmSciTech.* 17, 20–42. <https://doi.org/10.1208/s12249-015-0360-7>.
- Pfeifer, T., Koch, C., Van Hulle, L., 2016. Optimization of the FDM™ additive manufacturing process. *Proc. SPE ANTEC™ Indianap* 22–29.
- Skowrya, J., Pietrzak, K., Alhnan, M.A., 2015. Fabrication of extended-release patient-tailored prednisolone tablets via fused deposition modelling (FDM) 3D printing. *Eur. J. Pharm. Sci.* 68, 11–17. <https://doi.org/10.1016/j.ejps.2014.11.009>.
- Södergård, A., Stolt, M., 2002. Properties of lactic acid based polymers and their correlation with composition. *Prog. Polym. Sci.* 27, 1123–1163. [https://doi.org/10.1016/S0079-6700\(02\)00012-6](https://doi.org/10.1016/S0079-6700(02)00012-6).
- Torres, J., Cole, M., Owji, A., DeMastry, Z., Gordon, A.P., 2016. An approach for mechanical property optimization of fused deposition modeling with polylactic acid via design of experiments. *Rapid Prototyp. J.* 22, 387–404. <https://doi.org/10.1108/RPJ-07-2014-0083>.
- Turner, B.N., Strong, R., Gold, S.A., 2014. A review of melt extrusion additive manufacturing processes: I. Process design and modeling. *Rapid Prototyp. J.* 20, 192–204. <https://doi.org/10.1108/RPJ-01-2013-0012>.
- Tymrak, B.M., Kreiger, M., Pearce, J.M., 2014. Mechanical properties of components fabricated with open-source 3-D printers under realistic environmental conditions. *Mater. Des.* 58, 242–246. <https://doi.org/10.1016/j.matdes.2014.02.038>.
- Verreck, G., 2012. The Influence of Plasticizers in Hot-Melt Extrusion. *Hot-Melt Extrus. Pharm. Appl.* 93–112. <https://doi.org/10.1002/9780470711415.ch5>.
- Wang, S., Capoen, L., D'hooge, D.R., Cardon, L., D'hooge, D.R., Cardon, L., 2018. Can the melt flow index be used to predict the success of fused deposition modelling of commercial poly(lactic acid) filaments into 3D printed materials? *Plast. Rubber Compos.* 47, 9–16. <https://doi.org/10.1080/14658011.2017.1397308>.
- Wang, Y., Qin, Y., Zhang, Y., Yuan, M., Li, H., Yuan, M., 2014. Effects of N-octyl lactate as plasticizer on the thermal and functional properties of extruded PLA-based films. *Int. J. Biol. Macromol.* 67, 58–63. <https://doi.org/10.1016/j.ijbiomac.2014.02.048>.
- Xiao, L., Wang, B., Yang, G., Gauthier, M., 2012. Poly (Lactic acid) -based biomaterials: synthesis, modification and applications. *Biomed. Sci. Eng. Technol.* 249–283. <https://doi.org/10.5772/23927>.